Vehicle Parameter and Electric Powertrain Efficiency Analysis Using Real-Driving Data

Nico Rosenberger* and Markus Lienkamp
Institute of Automotive Technology, Technical University of Munich, Munich, Germany
Email: nico.rosenberger@tum.de (N.R.), lienkamp@tum.de (M.L.)

***Abstract*—With the conversion from Internal Combustion Engine Vehicles (ICEV) to Battery Electric Vehicles (BEV) mainly promoted by CO_2 emission targets, innovative powertrain concepts arose in the automotive industry. Original Equipment Manufacturers (OEMs) practice the so-called benchmarking to identify technological potentials in their competitor's concepts and reduce their development costs by focusing on the best-performing technologies in the electric vehicle market. In contrast, these analyses mean significant expenses in terms of time and cost. Especially on vehicle level, preparing the vehicles for dynamometer tests and performing multiple test series on these test benches require high personnel and time capacities. In this work, we present a methodology that reduces the effort of benchmarking analyses on vehicle level by substituting dynamometer tests. This methodology describes the identification of vehicle parameters and the analysis of the electric powertrain's efficiency. With no manipulation of the vehicle's structure and low-cost test equipment, data is recorded on public roads during real-driving scenarios, demonstrating our procedure's simplicity and universal application. With the obtained vehicle parameters (i.e. Road Load Coefficients (RLCs), rolling and air resistance) and the electric powertrain's efficiency map, we enable the parametrization of simulation models for further analyses. We validate our methodology based on tests performed on closed test tracks and a vehicle dynamometer.**

***Index Terms*—Controller area network, electric powertrain efficiency, real driving data, vehicle parameters**

I. Introduction

Within the *European Climate Law* passed in 2021, the European Union (EU) legally committed to achieving a net zero emission by 2050, intermediately targeting to reduce greenhouse gases (GHG) by 55% by 2030 compared to the level of 1990 [1]. In the European Scientific Advisory Board on Climate Change's report from 2023 [2], they identified the largest decarbonization potential in the conversion of light-duty vehicles (i.e. passenger cars) to BEV and their weight reduction since road transport accounts for 72% of the GHG within the transportation sector and light-duty vehicles contribute up to 61% of that share [3].

In this conversion from ICEV to BEV, many ideas and concepts for designing electric powertrains entered the market. Applying so-called "product benchmarking", OEMs aim to identify optimization potentials by analyzing products and innovative technologies yielded by competitors.

Although this process saves resources since OEMs no longer develop all concepts themselves, obtaining meaningful results from benchmarking remains cost and time-consuming. Whereas earlier studies [4, 5] focused on comparing single electric vehicles, more recent studies [6], [7] conducted comprehensive studies on multiple vehicles for several years, highlighting the effort for such benchmarking analyses. This effort is also shown by this research lab's work in two publications analyzing electric vehicles. Wassiliadis *et al.* [8] provided an in-depth analysis of the Volkswagen ID.3 Pro Performance on vehicle, component, and cell level. Later, we performed a similar in-depth analysis on the Tesla Model 3 Standard Range, focusing on vehicle level [9]. In both studies, the vehicles were prepared on closed test tracks, tested on a vehicle dynamometer for weeks, recording range data during official and real-driving-oriented drive cycles, conducting efficiency maps of the electric powertrains, and investigating the vehicle's behavior in charging scenarios. In contrast to the dynamometer tests, Komnos *et al.* [10] recorded data on public road measurements during real-driving scenarios to observe vehicle parameters. Besides avoiding expensive test bench measurements, expensive wheel force sensors were applied. The importance of a cost-efficient method to identify these parameters is described by Jamdade *et al.* [11], where a simulation model is used to predict vehicle performance and optimize energy management.

This study presents a methodology to design benchmarking processes that are more efficient and affordable. We present the concepts of identifying vehicle parameters and analyzing the electric powertrain's efficiency by observing real-driving data using affordable measurement equipment without manipulating the vehicle. Our work provides a universal approach for vehicle parameters and efficiency maps, allowing researchers to parameterize their simulation models and minimize the effort for those parameters.

To present this approach, the structure of this paper is organized as follows: Section II illustrates the design of experiment by introducing the vehicle under study, the measurement equipment, and the requirements of the test route. In Section III, we explain the concept of identifying the vehicle parameters and the results obtained from an

Manuscript received March 19, 2024; revised May 10, 2024; accepted June 15, 2024.
*Corresponding author

open-road test. Section IV follows analogously with the analysis of the electric powertrain's efficiency. Within Section V, our procedure is evaluated by comparing the open-road test results to the tests performed on a taxiway airfield and a vehicle dynamometer [8] before finally concluding the results in Section VI.

II. Design of Experiment

The introduction of the vehicle under study, the applied test equipment, and the test route requirements show this procedure's simplicity and universality.

A. Vehicle under Study and Test Equipment

The vehicle under study is the Volkswagen ID.3 1st Edition from 2020, the same vehicle as in [8], allowing us to evaluate our results in Section V. The required vehicle specifications are summarized in Table I, with the added mass m_r regarding the inertia of rotating parts calculated according to the Worldwide harmonized light vehicles test procedure (WLTP) regulations specified in [12].

$$m_r = 0.03 m_{\text{empty}} + 25\ \text{kg} \quad (1)$$

where m_{empty} describes the vehicle mass in running order given by the manufacturer in the certificate of conformity (CoC) according to EU Regulation 2018/858 [13].

TABLE I: SPECIFICATIONS OF THE VOLKSWAGEN ID.3 1ST EDITION

Domain	Attribute	Value	Unit
Vehicle	Range (WLTP)[c]	408	km
	Max. Speed[c]	160	km/h
	Tyres[c]	215/45 R20 95T	-
	Tyre radius[m]	346.8	mm
	RLC – f_0[c]	110.0	N
	RLC – f_1[c]	0.855	N/(km/h)
	RLC – f_2[c]	0.02445	N/(km/h)^2
	Air res. coefficient[a]	0.267	-
	Rolling res. coefficient[l]	0.008	-
Power unit	Max. power[c]	150	kW
	Cont. power (30 min)[c]	70	kW
	Max. rotations[a]	16,000	rpm
	Max. torque[c]	310	Nm
	Drive type[a]	PSM	
	Inverter[a]	IGBT	
	Gearing ratio[c]	11.53:1	-
Test masses	Empty mass m_{empty}[c]	1794	kg
	Actual mass m[c]	1891	kg
	Added mass m_r[l]	78.82	kg
	Test mass m_{test}[m]	1937.5	kg
	Total test mass m_{tot}[m]	2016.3	kg

[m] Determined by measurements.
[c] Taken from the CoC and the vehicle registration documents.
[l] Taken from literature [12, 14].
[a] Assumptions taken from media and press releases [15].

The equipped measurement technology consists of two devices: A data logger recording the Controller Area Network (CAN) data and an Inertial Navigation System (INS) recording vehicle dynamics. The CAN logger developed at our institute and introduced by Merkle *et al*. [16] is connected at the onboard diagnostics (OBD)-II port. This tool sends requests and receives responses via the Unified Diagnostics Service (UDS) protocol. The recorded signals are mostly the same as [8], besides some additional signals necessary for open-road tests.

The second part of the measurement equipment is an RT2500 (Oxford Technical Solutions Ltd., United Kingdom), which is additionally connected to a Global Positioning System (GPS)-antenna. The RT2500 is an INS recording high-precision measurements in an easy operation. This system records translational and rotational positions of the vehicle in different reference systems and their respective velocities and accelerations. Table II provides the signals of both measurement devices.

TABLE II: OVERVIEW OF THE CAN AND THE INS SIGNALS

Domain	Signal name (unit)	Vehicle parameter	Powertrain efficiency
CAN	time (UTC time | ms)	X	X
	hv_battery_current (A)		X
	hv_battery_voltage (V)		X
	hvlv_aux_power (W)		X
	axle_torque_nominal (Nm)	X	X
	engine_rpm (rpm)	X	X
	steering_wheel_angle (°)	X	
	brake_pedal_activated (-)	X	
	gear_selected (-)	X	
INS	Time (GPS | ms)	X	
	UTC offset (s)	X	
	Speed 3D with hold (m/s)	X	
	Pitch misalignment angle (°)	X	
	Pitch (°)	X	
	Heading (°)	X	

Signals of the CAN communication, recorded via UDS.
Signals of the INS, recorded via GPS on RT2500.

Whereas the GPS antenna does not require special mounting, the RT2500 must be firmly attached to prevent relative motion between the vehicle and the device. The GPS antenna is installed inside the vehicle to prevent a negative impact on the vehicle's air resistance.

Our measurement setup is low-cost and easy to operate. Our procedure grants easy access to the vehicle's internal data without manipulating the production status of the vehicle. By only requesting the necessary signals, we can ensure a sampling rate of 10 Hz. Also, the mounting of the INS is adaptable and thus enables the application in multiple vehicles.

B. Test Route Requirements

With the following test route requirements, we secure reproducible and representative results even though this investigation is based on real-driving data on open roads. This leads to general and specific requirements regarding the test route, the climate, and further test conditions.

To start with the general requirements, multiple straights are required for our driving resistance observations, with both high-speed sections allowing us to reach the vehicle's top speed and low-speed sections allowing the vehicle to stop. Charging stations within a certain proximity to the route are beneficial. With a tool that displays the most suitable route based on the defined boundary conditions, we ensure a universal approach independent of the respective location. Before the measurement starts, the vehicle is brought to operation conditions.

Specific requirements for the identification of the vehicle parameters are described as follows: The test route must not have a sudden inclination change. Continuous

inclinations, in contrast, will be handled. In this investigation, straight sections are crucial to limit the necessary steering interventions. Road surface conditions must meet representative characteristics of public roads [12]. Based on the official test procedure in [12], Sarkan *et al*. [17] derived test conditions for an official coast-down test. The most significant requirements are wind velocities of <5 m/s, a dry road surface, and air temperatures between 5 ℃ and 40 ℃. Further test requirements are that all vehicle windows remain closed, only small to no steering interventions are allowed during coast-down segments, and traffic needs to be monitored precisely. Preceding vehicles might affect the air resistance and, thus, the results of a coast-down measurement. In case of a closing vehicle, the recording must be stopped immediately. Instead of using a certain signal (i.e. adaptive cruise control (ACC)), recordings will be stopped by either using the brake pedal or switching gears since ACC is not integrated into all vehicles. Also, to reach representative results, we repeat our route in the described sections to record multiple coast-downs in both directions following [17].

For the requirements of the electric powertrain's efficiency analysis, rather than the sheer amount of data, the focus is to reach every operating point within the boundaries of the vehicle. In contrast to the vehicle dynamometer, we cannot hold certain operating points to reach steady-state behavior and record the efficiency. In real-driving scenarios, operating points are rather passed through. Thus, conclusive results are achieved through repetition. During test drives, measurements can be stopped and restarted multiple times (e.g. during charging processes). In addition, air conditioning or cabin heating is turned off.

III. Identification of Vehicle Parameters

The identification of the vehicle parameters, including identifying valid coast-down segments, conflating those to vehicle resistance forces, and elaborating the vehicle parameters, replaces expensive closed-road tests.

A. Fundamentals and Methodology

First, the vehicle's gear must be switched into neutral (N) to identify potential coast-down segments. The brake pedal stops valid segments, which might also be targeted (i.e. closing preceding vehicles). Segments before and after brake pedal activation might remain valid if these last longer than a minimum velocity difference of Δv_{min}=10 km/h. Inclinations leading to positive accelerations must not be considered. The continuity of an inclination is determined by a threshold value of ±0.15 %. Also, only small steering interventions (< ±5) permit valid segments. Heading information secures segments in both directions.

Fig. 1 displays our approach, oriented on the official procedure for conducting coast-down segments [12]. Every valid segment is examined for all velocity sections. For example, in the figure, the two blue segments (points 1 & 2) belong to the displayed reference velocity since they start and end outside this section. This does not apply to the green and orange segments (points 3 & 4).

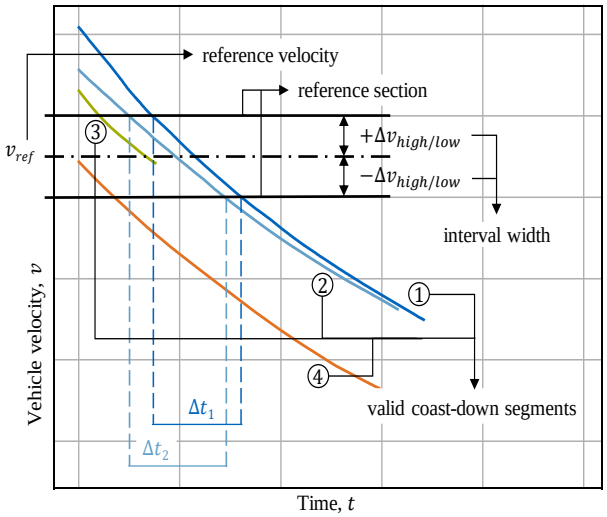

Fig. 1. Overview of the procedure to analyze the coast-down segments with a reference velocity v_{ref}, an interval width $\pm\Delta v_{\text{high/low}}$, and a reference section with in- and excluded segments.

A reference section is defined by the reference velocity v_{ref} and reference interval width $\pm\Delta v_{\text{high/low}}$. United Nations [12] specifies the requirements as a minimum of six reference sections need to be considered, and the velocity gap between two reference velocities must not exceed 20 km/h. The interval width of low reference velocities (≤ 60 km/h) must not exceed a threshold value of Δv_{low} = 5 km/h, whereas higher reference velocities (> 60 km/h) must not exceed a threshold value of Δv_{high} = 10 km/h. To comply with these requirements, in this study, we conduct 31 reference velocities between $v_{\text{ref,min}}$ = 5 km/h, and $v_{\text{ref,max}}$ = 150 km/h (constant internal of Δv_{ref} = 5 km/h), and with interval widths of Δv_{low} = 5 km/h and Δv_{high} = 10 km/h, ensuring all requirements are met.

The time difference Δt obtained from the procedure is defined for all valid segments, and the acceleration force $F_{\text{acceleration}}$ is calculated within the respective reference section $2\Delta v_{\text{high/low}}$.

$$F_{\text{acceleration}} = m_{\text{tot}} a = (m_{\text{test}} + m_{\text{r}}) \frac{2\Delta v_{high/low}}{\Delta t}. \quad (2)$$

m_{tot} and m_{test} yield the calculated total and measured test mass given in Table I. Since continuous inclination is included, the inclination force $F_{\text{inclination}}$ is considered as:

$$F_{\text{inclination}} = m_{\text{test}} g \sin \alpha, \quad (3)$$

where α represents the recorded angle of inclination from the INS. The overall resistance force $F_{\text{resistance},j}$ of section j is calculated using

$$F_{\text{resistance},j} = \frac{1}{N}\left[\sum_1^N \left(-F_{\text{acceleration},ij} - F_{\text{inxlination},ij}\right)\right], \quad (4)$$

where the difference of the forces to a segment i in the reference section j builds the resistance force $F_{\text{resistance},ij}$. Besides the resistance force, the air density is used to calculate the vehicle parameters. With the mean of all segments within a reference velocity, the overall resistance force $F_{\text{resistance},j}$ and air density $\rho_{L,j}$ of every section j are compiled.

The resulting means at every reference velocity are fitted into one resulting coast-down curve by applying the Levenberg-Marquardt algorithm [18]. This algorithm is a nonlinear least-square method and the standard procedure for fitting such a curve according to [10, 12]. The result of this algorithm is described by:

$$F_{\text{resistance},j} = f_0 + f_1 v_j + f_2 v_j^2, \quad (5)$$

where f_0, f_1, and f_2 represent the road load coefficients [19] and v_j the respective reference velocities. For the vehicle parameters (i.e. rolling and air resistance), we present two approaches: in the first one, the vehicle parameters are conducted similarly to the RLCs but applying:

$$F_{\text{resistance},j} = m_{\text{test}} g f_R + \frac{1}{2} \rho_{L,j} A_{\text{front}} c_W v_j^2, \quad (6)$$

where A_{front} describes the vehicle's frontal area, f_R is the targeted rolling resistance, and c_W is the air resistance coefficient. The second approach identifies the vehicle parameters based on the RLCs and not on the vehicle resistances or the coast-down curve. This approach is applied when only RLCs are given.

B. Open-Road Test Results

The results of the real-driving test with the filtered coast-down segments are illustrated in Fig. 2. During the open-road test with a duration of t = 5.4 h, 82 coast-down segments were recorded. After all filters were applied, 89 segments were considered valid. The higher number of valid segments compared to the recorded ones can be explained by point 3. If invalid segments are identified, segments before and after might remain valid if they exceed the minimum velocity difference of Δv_{min} = 10 km/h. This results in increasing valid segments compared to the recorded ones. The invalid segments are rooted in brake pedal activation (point 1), increasing acceleration due to downhill driving (point 2), and changing inclinations and steering interventions (point 3).

Although the valid segments show similar curve characteristics, some differ in their respective gradient as a result of allowing continuous inclinations, which are considered through (3). For lower reference velocities, the segments present diverging behavior.

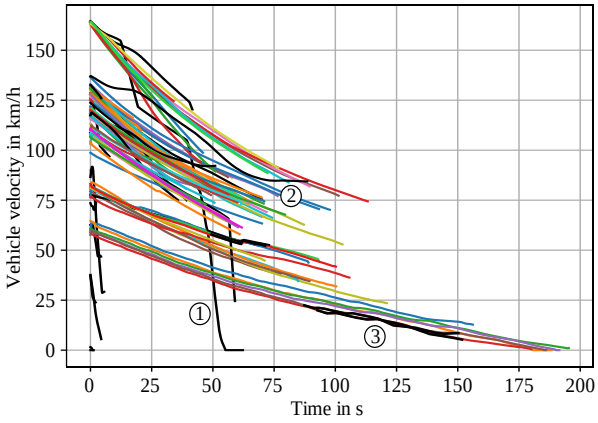

Fig. 2. Overview of all recorded coast-down segments with invalid segments marked black. All colored segments are examined in all reference sections.

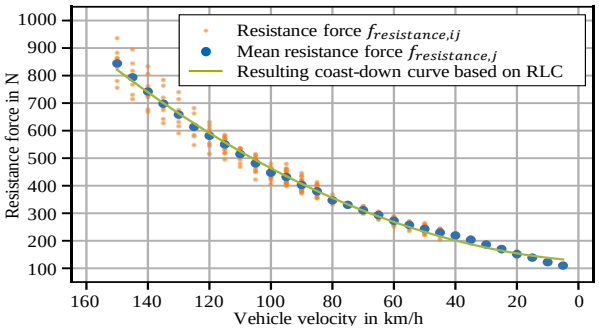

Fig. 3. Fitted coast-down curve to the RLCs with the respected mean resistance forces calculated considering the valid segments at all reference velocities.

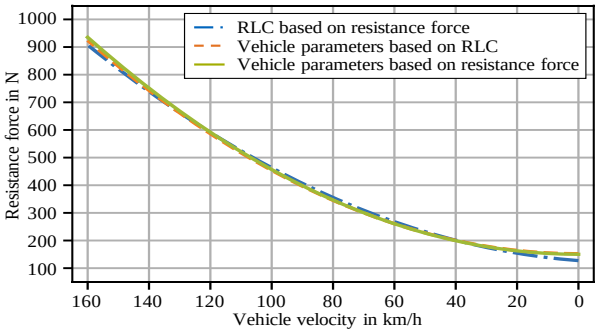

Fig. 4. Coast-down curve results fitted considering the road load coefficients (blue), the vehicle parameters based on the RLCs (orange), and the vehicle parameters based directly on the resistance forces (green).

The resistance forces for every included segment in the respective reference section (orange points) are illustrated in Fig. 3. The variation of these resistance forces rises with higher reference velocities, as does the number of included segments. The bigger blue points represent the mean of the respective resistance forces. Applying the fitting algorithm regarding (5), we observe the green curve as an overall coast-down curve.

This curve is represented by the road load coefficients of f_0 = 127.3 N, f_1 = 0.83 N/(km/h) and f_2 = 0.02529 N/(km/h)^2. The fitting to these parameters results in a root mean square error (RMSE) of 11.07. Following the graph to descending reference velocities, the curve fits the velocities at higher vehicle speeds comparably well until a reference velocity of v_{ref} = 60 km/h. Lower vehicle speeds show significant deviations in both directions. Fig. 4 shows the results of the two approaches for the vehicle parameter identification compared to the coast-down curve generated through the road load coefficients in the previous figure.

Comparing the results from the RLCs (blue) to the derived vehicle parameters based on the RLCs (orange), we observe deviations regarding the curvature, especially at lower vehicle speeds. The rolling resistance is modeled as a constant for the vehicle parameters, whereas, in the RLCs, it is modeled as a partly constant and partly velocity-dependent parameter. Comparing the derived vehicle parameters based on the RLCs to the parameters directly fitted to the resistance forces applying (6) (green), we identify an overall similar characteristic except around top speed with the directly fitted curve reaching higher resistance forces, and thus, reaching higher deviations compared to the RLCs curve.

IV. Analysis of Electric Powertrain Efficiency

Analogously to the structure in Section III, after introducing the concept for the powertrain efficiency analysis, the electric powertrain's efficiency results confirm that vehicle dynamometer testing can be saved.

A. Fundamentals and Methodology

This study focuses on the electric power unit consisting of the power electronics, electric machine, and transmission. The starting point is the electric power out of the battery into the power electronics. Still, considering the electrical power into the high and low voltage auxiliaries, the remaining power into the power electronics is considered the input power.

The output power is described by the mechanical power obtained on the powered axle of the vehicle. In contrast, this test procedure is easily adapted if the focus is on specific components. For example, when focusing only on the electric machine's efficiency or when a simulation model is built with every component included, single efficiencies can be obtained by recording the respective power into and off the component under study. Thus, for comparability to the results from [8], we focus on the electric power unit as one unit. Also, we focus on the upper right quadrant (positive motor speed and positive torque), whereas fundamentally, every quadrant is possible with this procedure. The power distribution is given by:

$$P_{\text{Power unit,in}} = P_{\text{Battery,out}} - \left(P_{\text{Aux LV,in}} + P_{\text{Aux HV,in}}\right) = P_{\text{Battery,out}} - P_{\text{Aux,in}}, \quad (7)$$

where P describes the power and the indices the direction of the power of the respective components. The signal in Table II combines high and low voltage auxiliaries. Since all signals up to the electric machine are electrical, power is given by their respective currents and voltages.

$$P_{\text{component,in/out}} = V_{\text{component,in/out}} \cdot I_{\text{component,in/out}}, \quad (8)$$

where V represents voltages and I currents off or into the described components. The output power is the mechanical power obtained on the vehicle's powered axle or off the transmission.

$$P_{\text{Power unit,out}} = T_{\text{Transmission,out}} \cdot \omega_{\text{Transmission,out}}, \quad (9)$$

where T describes the mechanical torque and ω the angular velocity.

The identification of the efficiency map starts with its upper boundary, the full-load characteristic, which is the maximum amount of torque at a specific motor speed. Within this curve, characteristic points are evaluated, such as the rated torque T_{rated} describing the maximum torque, the base speed n_{base} specifying the maximum speed T_{rated} is available, and the maximum speed n_{max} itself. With the full-load characteristics, the area under this curve is structured in a grid. Stockman *et al.* [20] proposed a grid with an interval of 19 for the vehicle speed and 16 for the torque, where the resulting nodes build the center points. In this study, we selected the same grid as in [8] for comparability.

This led to a velocity-depending grid, where the number of nodes in the area of lower rotational speeds ($n \leq 2160$ rpm) is increased. Every node creates an area of corresponding measurement points. This area is both torque- and speed-dependent. the interval width for lower torques ($T_{\text{threshold}} \leq 31$ Nm) is set to $\pm\Delta T_{\text{low}} = 10$ Nm, whereas it increases to $\pm\Delta T_{\text{high}} = 15$ Nm for higher torques. Analogous to the torque, the interval width of the rotational speed increases from $\pm\Delta n_{\text{low}} = 300$ rpm to $\pm\Delta n_{\text{high}} = 600$ rpm at the threshold of $n_{\text{threshold}} \leq 2800$ rpm. The corresponding maximum torque is taken from the full-load curve for every speed within the interval to cut the grid at these nodes. In addition, the characteristic points are also considered to precisely follow the upper boundary and to ensure inter rather than extrapolation at all times.

For every area around those nodes, we determine the mean value of the power unit's efficiency, the standard deviation, and the range. We calculate the trimmed mean for efficiency to reduce the impact of outliers [21]. The Standard deviation and range are mainly conducted to verify the validity of our proposed procedure and compare it to steady-state behavior on a vehicle dynamometer. This observation led to the condition that within the area of more frequent nodes ($n \leq 2160$ rpm), a minimum of 20 measurement points must be available. In contrast, a minimum of 100 measurement points secure an average behavior for wider spread nodes.

To complete the efficiency map, we connect the nodes through linear interpolation based on [22] as the standard procedure following several studies [20, 23]. Comparably to the final efficiency map in [8], where the torque could not be set precisely at every speed level, the nodes in this study also do not exactly follow the grid since the mean values depend on the measurement points within the areas.

B. Real-Driving Scenario Results

Now, we present the resulting efficiency map following our procedure. First, we analyze this efficiency map, and later, in Section V-B, this result is compared to the efficiency map through the dynamometer test. Fig. 5 illustrates the result of our test drive with a duration of $t = 4.2$ h. The white crosses in the efficiency map display all nodes with the required number of measurement points.

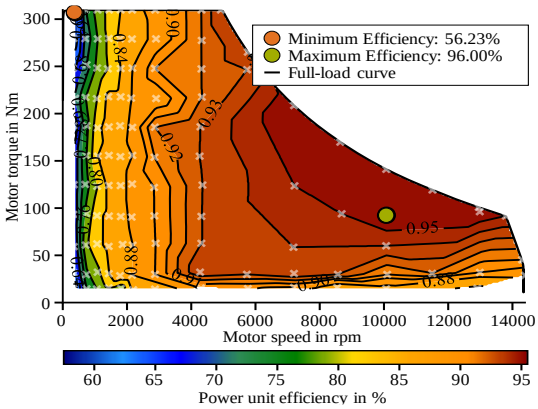

Fig. 5. Resulting efficiency map with the full-load curve (black) as the upper boundary, the location of the minimum efficiency (orange), and its maximum efficiency (green).

In this figure, the full-load curve presents the characteristics of the electric machine. The rated torque of

T_{rated} = 309.75 Nm is available until the base speed of $n_{base} \leq 4921$ rpm. The torque decreases progressively to a final value of T_{nmax} = 49.8 Nm, which is reached at the maximum speed of n_{max} = 14,390 rpm. In contrast to the general torque characteristics of electric machines, we observe a kink at the rotational speed of n = 14,064 rpm, where the maximum torque massively decreases up to the maximum speed. This behavior is due to the electronic limit of v_{max} = 160 km/h. The green point close to the full-load curve and at higher rotational speeds marks the maximum efficiency of η_{max} = 96.00 %. In contrast, the minimum efficiency of η_{min} = 56.23 % is reached at low rotational speeds close to zero but high demand of torque. Note that this efficiency not only represents the electric machine but the whole power unit, including power electronics and transmission. The standard deviations are an indicator of the range of the measurement points. We must accept a certain range since we include an area around the nodes rather than recording the vehicle's behavior at a specific node (like on a vehicle dynamometer). The results show greater deviations at lower speeds, but standard deviations of $\sigma \leq 2\%$ are reached over most of this efficiency map.

V. Evaluation

Finally, the results are compared to the considerably official test procedures. In addition to a direct comparison, we will discuss the impact of their deviations on potential further analyses using a simulation model calculating the WLTP range.

A. Evaluation of the Identification of Vehicle Parameters

The comparison of the coast-down segments of our open-road data set to the tests performed on a closed runway of an airfield [8] and provided data by the manufacturer in the CoC starts with the road load coefficients from Section III-B. Fig. 6 presents the coast-down curves generated using the RLCs. The curve recorded on a closed-road test differs in its characteristics compared to the curve generated from the data on the open-road test. Although its maximum resistance force is smaller than the open-road result, its resistance close to stillstand is almost equal due to its smaller gradient.

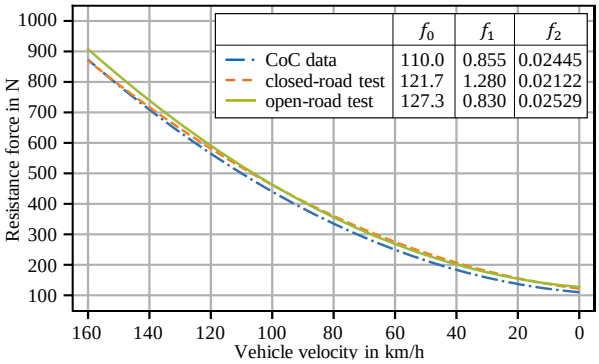

Fig. 6. Coast-down results of official data given in the CoC (blue), data recorded on a closed airfield (orange), and through open-road measurements (green).

The official data provided by the manufacturer presents far more similar results to the open-road tests regarding its characteristics than the results from the airfield. Although its shape is nearly identical, the open-road results appear to have an offset since the gap between the two curves seems constant. This results from a higher velocity-independent coefficient f_0. Different vehicle test masses likely cause this difference. In recent studies, similar results were obtained regarding higher velocity-independent coefficients and, thus, higher driving resistances at all velocities [10, 24]. Another potential reason might be tire treatments before the official tests the manufacturer performs. We secured the official tire pressure recommendation and warmed up the tires before the recording. Comparing the parameters, f_0 is similar between the airfield and the open-road test, which might indicate similar test masses. Considering the road inclination allows us to reach a more accurate and recording data on different road surfaces a more average result compared to the test on the closed test track.

The simulation model determining the impact of the deviations of the results calculates the WLTP range based on the RLCs with the following boundary conditions: The efficiency is set to $\eta = 1$ since we focus on the vehicle parameters, not the vehicle's efficiency. In addition to the constant efficiency, we used the test masses of the respective test procedures for the considered vehicle mass. Table III provides the WLTP ranges of the CoC data, the closed-road, and the open-road tests from this study.

Table III: WLTP Ranges Based on the RLCs and their Deviation

Test Procedure	WLTP Range	Deviations from CoC data
CoC data	471.59 km	-
closed-road test	456.39 km	−3.2 %
open-road test	461.16 km	−2.2 %

The manufacturer's results provide the highest range consistent with the results from Fig. 6. Even though the closed-road tests achieve comparable resistances at higher speeds, the achieved range is the lowest. This is rooted in the lower shares of high-speed driving in the WLTP. The range of our proposed test procedure is closer to the official with a deviation of only 2.2%. Also, closed- and open-road test results differ by only 1%.

Furthermore, when transferring the RLCs to vehicle parameters, we can compare the closed-road and manufacturer's test results with the vehicle parameters from our procedure. This also explains the two approaches for the vehicle parameters since we can only rely on the RLCs for those tests and not on the actual coast-down results. Table IV presents the different vehicle parameters for the rolling and air resistance according to the respective tests. In addition, official data provided by the manufacturer [15] and a rough reference value for the rolling resistance described in [14] are included as references.

Comparing the manufacturer's derived results to their air resistance and a potential rolling resistance shows the difficulty in their comparison since the result is based on their combination and not separately determined. The manufacturer did not publish a result for the rolling

resistance. Thus, we will focus on the air resistance. Both of the manufacturer's values for the air resistance present quite a high deviation of nearly 5%. The air resistance of the closed-road test is in between the two results, whereas the result of the open-road test appears to be higher.

TABLE IV: WLTP RANGES BASED ON VEHICLE PARAMETERS AND THEIR DEVIATION

Test Procedure	Resis. coeff.		WLTP Range	Deviations CoC data
	c_W	f_R		
CoC data[RLC]	0.280	0.0070	482.64 km	-
closed-road test[RLC]	0.273	0.0083	466.88 km	−3.3 %
open-road test[RLC]	0.286	0.0080	463.57 km	−4.0 %
open-road test[VP]	0.291	0.0079	461.30 km	−4.4 %
official data[a]	0.267	0.008	476.37 km	−1.3 %

RLC Based on (5); VP Based on (6).

[a] Assumptions taken from literature [14, 15].

The table also provides the simulation model results applying the combination of both parameters. Comparing the results of the WLTP range to the manufacturer's parameters based on the RLCs, the manufacturer's air resistance and the literature-based rolling resistance come closest. All parameter combinations derived from road tests differ significantly from the manufacturer's data. Especially the vehicle parameters, even though the two approaches almost match, derived based on the direct approach deviate with a total of 4.4% the highest. Comparing the results of the closed- to the open-road tests, both derived based on the RLCs differ only about 0.7% and a total of 3.3 km. We did not aim to improve the test procedure compared to closed-road tests but rather void expensive test track time and maintain the measurement quality. This result approves our proposed test procedure, and thus, open-road tests are admissible for the road load coefficients and for the identification of vehicle parameters.

B. *Evaluation of the Analysis of the Electric Powertrain Efficiency*

Last, we superimpose the efficiency map conducted during real-driving scenarios to the efficiency map recorded on the vehicle dynamometer. Fig. 7 presents the overlay of the two efficiency maps based on the dynamometer and the real-driving tests. The overall light appearance confirms similar efficiency maps, especially beneath the full-load curve with deviations between $\Delta\eta < 2\%$.

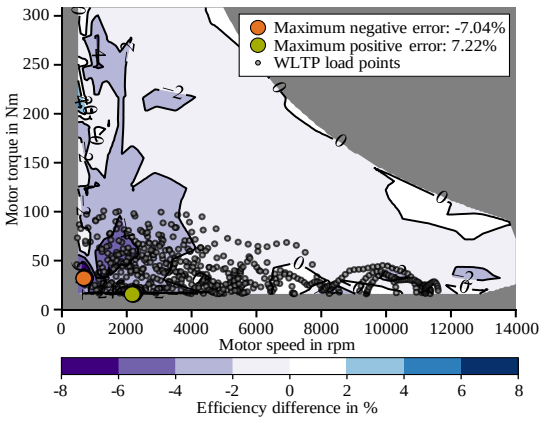

Fig. 7. Efficiency map overlay between the vehicle dynamometer test [8] and the data obtained from the real-driving scenario.

The greatest deviations appear at lower speeds throughout the whole torque interval. Whereas purple areas indicate higher efficiencies in the real-driving results, blue areas present lower efficiencies than in the dynamometer test. The only darker areas appear in the low-torque and low-speed area, where maximum deviations of around $\Delta\eta_{max} = 7\%$ are reached, resulting in a mean difference $\Delta\eta_{mean} = 1.41\%$.

Similar to the simulation model presented before, we apply these efficiency maps to a model to quantify their impact on further range analyses. The grey points in the figure represent the load points of the WLTP driving cycle. Since these points mostly cover the area of lower torque demand, the WLTP is applied to areas of lower accordance. Note that we do not include the load points in the grey area ($T < 15$ Nm & $n < 400$ rpm) since no data is available in the overlay efficiency map. Since neither efficiency map analyzes the fourth quadrant (positive motor speed & negative torque), we will not include regenerative braking efficiency.

Considering these assumptions for our simulation model, a significantly increased WLTP range is given compared to the CoC range. That also applies to the results of the road load coefficients and the vehicle parameters; different simulation models were implemented, and thus, results must not be compared. Table V shows the results regarding the WLTP range of the simulation model compared to a model of $\eta = 1$.

TABLE V: WLTP RANGES BASED ON THE ELECTRIC POWERTRAIN'S EFFICIENCIES

Test Procedure	WLTP Range	Deviations from $\eta = 1$
optimal model ($\eta = 1$)	471.59 km	-
dynamometer test	435.59 km	7.6 %
real-driving test	427.37 km	9.4 %

Focusing not on the efficiency results quantitatively but rather on approving the proposed test procedure, the real-driving test range of $s_{\text{real-driving}} = 427.37$ km deviates by only 8.2 km (1.9%) compared to the range of the dynamometer test of $s_{\text{dynamometer}} = 435.59$ km. Note that the WLTP load points are mainly located in areas of greater deviation. Analogously to the RLCs and vehicle parameter results, the efficiency comparison also approves the proposed procedure. This saves the cost of operating the dynamometer and greatly reduces testing time.

VI. CONCLUSION

This study presents an efficient and affordable process to identify vehicle parameters and analyze the powertrain efficiency of an electric vehicle. Explaining the concept with all required mathematical foundations and parameter boundary conditions, we describe our procedure in detail, and by comparing the results to official test procedures, we prove the validity of our procedure.

Universal validity is given by the equipment and the utilized signals by performing measurements on public roads and not manipulating the vehicle under study. Time and cost are saved compared to expensive test procedures on vehicle dynamometers and closed test tracks.

The identification of the road load coefficients, rolling, and air resistance proved that open-road tests are legitimate, comparing the results to the closed-road tests. Through the WLTP simulation, we proved the differences in further analysis are marginal, with only 1% between open- and closed-road test results. The electric powertrain's efficiency analysis has been approved by comparing it to the results obtained from the vehicle dynamometer. Whereas the efficiency maps mostly present an overlay difference of $\Delta\eta < \pm 2\%$, even areas with greater differences (lower torque or lower speed) do not exceed $\Delta\eta = 7.22\%$. Although the WLTP cycle targets areas of greater difference (lower torque), this procedure is confirmed by reaching a difference in the total range of 1.9%.

The future work resulting from this study is to further increase the accuracy in areas of higher differences. This might be achieved with more data, especially focusing on these areas. Regarding the vehicle parameters, in future work, it would be beneficial to analyze the rolling and air resistance separately. Last, we are working on an automation method for the reverse engineering of the CAN communication of the vehicle under study to enable researchers without previous knowledge or experience access to the signals.

CONFLICT OF INTEREST

The authors declare no conflict of interest.

AUTHOR CONTRIBUTIONS

Nico Rosenberger is the primary researcher of this work and the main author of this study. Markus Lienkamp provided scientific advisory. All authors had approved the final version.

FUNDING

This work was funded by the German Federal Ministry for Economic Affairs and Climate Action (BMWK) within the project "ScaleUp-eDrive" under grant number 16THB0006C.

REFERENCES

[1] European Union Council, Regulation (EU) 2021/1119 of the European Parliament and of the Council of 30 June 2021 establishing the framework for achieving climate neutrality and amending regulations (EC) no 401/2009 and (EU) 2018/1999 ('European Climate Law'). (2024). [Online]. Available: http://data.europa.eu/eli/reg/2021/1119/oj

[2] European Environment Agency, *Scientific Advice for the Determination of an EU-Wide 2040 Climate Target and a Greenhouse Gas Budget for 2030–2050*, Publications Office of the European Union, 2023.

[3] European Environment Agency, *Transport and Environment Report 2021: Decarbonising Road Transport—the Role of Vehicles, Fuels and Transport Demand*, Publications Office of the European Union, 2022, no. 02/2022.

[4] K. J. Kelly and A. Rajagopalan, "Benchmarking of OEM hybrid electric vehicles at NREL: Milestone report," *National Renewable Energy Laboratory*, Dec. 2001.

[5] L. Eckstein, R. Gobbels, and R. Wohlecker, "Benchmarking of the electric vehicle mitsubishi I-Miev," *ATZautotechnology,* 2011. doi.org/10.1365/s35595-011-0078-4.

[6] G. Oh, D. J. Leblanc, and H. Peng, "Vehicle Energy Dataset (VED), a large-scale dataset for vehicle energy consumption research," *IEEE Trans. on Intelligent Transportation Systems*, 2020. doi.org/10.48550/arXiv.1905.02081

[7] J. Diez, "Advanced vehicle testing and evaluation, final technical report encompassing project activities from October 1, 2011 to April 30, 2018," Intertek Testing Services, NA, Inc., Arlington Heights, IL (United States), Tech. Rep. 2018. doi.org/10.2172/1481912.

[8] N. Wassiliadis, M. Steinstr äter, M. Schreiber *et al.*, "Quantifying the state of the art of electric powertrains in battery electric vehicles: Range, efficiency, and lifetime from component to system level of the Volkswagen ID.3," *eTransportation*, 2022. doi.org/10.1016/j.etran.2022.100167

[9] N. Rosenberger, P. Rosner, P. Bilfinger *et al.*, "Quantifying the state of the art of electric powertrains in battery electric vehicles: Comprehensive analysis of the Tesla Model 3 on the vehicle level," *World Electr. Veh. J.*, 2024. doi.org/10.3390/wevj15060268

[10] D. Komnos, S. Broekaert, N. Zacharof, L. Ntziachristos, and G. Fontaras, "A method for quantifying the resistances of light and heavy-duty vehicles under in-use conditions," *Energy Conversion and Management*, 2024. doi.org/10.1016/j.enconman.2023.117810

[11] A. Jamdade, M. H. Jalali, M. Savoy and K. Bubbar, "High-fidelity modelling, parameter identification, and co-simulation of a 4-wheel independent drive and steer electric vehicle with custom inverter design," in *Proc. 2023 Int. Conf. on Control, Automation and Diagnosis*, 2023. doi: 10.1109/ICCAD57653.2023.10152448

[12] United Nations. Global technical regulation on Worldwide harmonized Light vehicles Test Procedure. Addendum 15: Global technical regulation No. 15 (ECE/TRAN/180/Add.15). (2024). [Online]. Available: https://unece.org/fileadmin/DAM/trans/main/wp29/wp29r-1998agr-rules/ECE-TRANS-180a15e.pdf

[13] European Parliament. Regulation (EU) 2018/858 of the European Parliament and of the Council of 30 May 2018 on the approval and market surveillance of motor vehicles and their trailers, and of systems, components and separate technical units intended for such vehicles, amending Regulations (EC) No 715/2007 and (EC) No 595/2009 and repealing Directive 2007/46/EC. (2024). [Online]. Available: https://eur-lex.europa.eu/eli/reg/2018/858/oj

[14] H. Naunheimer, B. Bertsche, J. Ryborz, W. Novak, and P. Fietkau, *Fahrzeuggetriebe: Grundlagen, Auswahl, Auslegung und Konstruktion*, Springer Vieweg Berlin, Heidelberg, 2019.

[15] Volkswagen. technische Daten des VW ID 3. (2024). [Online]. Available: https://www.vw-id3.info/de/technische-daten

[16] L. Merkle, M. Pothig, and F. Schmid, "Estimate e-Golf battery state using diagnostic data and a digital twin," *Batteries*, 2021. doi.org/10.3390/batteries7010015

[17] B. Sarkan, T. Skrucany, S. Semanova, R. Madlenak, A. Kuranc, M. Sejkorova, and J. Caban, "Vehicle coastdown method as a tool for calculating total resistance for the purposes of type-approval fuel consumption," *Scientific Journal of Silesian University of Technology*, 2018. doi.org/10.20858/sjsutst.2018.98.15

[18] K. Levenberg, *A Method for the Solution of Certain NonLinear Problems in Least Squares*, Brown University, 1944.

[19] Green NCAP. Test procedure: Driving Resistance. (2019). [Online]. Available: https://www.greenncap.com/wp-content/uploads/GNT_Driving_Resistance v1.0.0.pdf

[20] K. Stockman, S. Dereyne, D. Vanhooydonck, W. Symens, J. Lemmens, and W. Deprez, "Iso efficiency contour measurement results for variable speed drives," in *Proc. The XIX International Conference on Electrical Machines*, 2010, pp. 1–6. doi.org/10.1109/ICELMACH.2010.5608035

[21] R. R. Wilcox and K. H. J, "Modern robust data analysis methods: measures of central tendency," *Psychol Methods*, 2003. doi.org/10.1037/1082-989x.8.3.254

[22] B. Barber, D. Dobkin, and H. Huhdanpa, "The quickhull algorithm for convex hulls," *ACM Trans. on Mathematical Software*, vol. 22, no. 4, pp. 469–483, 1996. doi.org/10.1145/235815.235821

[23] C. Depature, W. Lhomme, A. Bouscayrol, L. Boulon, P. Sicard, and T. Jokela, "Characterisation of the electric drive of EV: on-road versus off-road method," *IET Electrical Systems in Transportation*, vol. 7, pp. 215–222, 2017. doi.org/10.1049/iet-est.2016.0060

[24] G. Kadijk and N. Ligterink. TNO 2012 R10237: Road load determination of passenger cars. (2012). [Online]. Available:

https://www.tno.nl/media/1971/road_load_determination_passenger_cars_tno_r10237.pdf.

Nico Rosenberger was born in Aschaffenburg on October 19, 1995. He studied mechanical engineering at the Technical University of Darmstadt, and earned his bachelor's and master's degrees in 2018 and 2021, respectively. Since 2022, he has been employed at the Institute of Automotive Technology (FTM) at the Technical University of Munich (TUM). His primary research interest is the analysis of battery electric vehicle concepts and optimizing electric powertrains.

Markus Lienkamp was born in 1967. He studied mechanical engineering at the Technical University of Darmstadt (TUD) and Cornell University, and obtained his doctorate at TUD in 1995. He worked at Volkswagen as part of an international trainee program and took part in a joint venture between Ford and Volkswagen in Portugal. Returning to Germany, he led the brake testing department in the VW commercial vehicle development section in Wolfsburg. He later became head of the "Electronics and Vehicle" research department in Volkswagen AG's Group Research division. Prof. Lienkamp has been the professor of the FTM at TUM since November 2009.